Asymmetric Cathodoluminescence Emission in $CH_3NH_3PbI_{3−x}Br_x$ Perovskite Single Crystals

M. Ibrahim Dar,*[†,#] Gwénolé Jacopin,[‡,#] Mahmoud Hezam,[‡,||] Neha Arora,[†,§]
Shaik Mohammed Zakeeruddin,[†] Benoit Deveaud,[‡] Mohammad Khaja Nazeeruddin,[§]
and Michael Grätzel[†]

[†]Laboratory of Photonics and Interfaces, Institute of Chemical Sciences and Engineering, [‡]Laboratory of Quantum Optoelectronics, Institute of Physics, and [§]Group for Molecular Engineering of Functional Materials, Institute of Chemical Sciences and Engineering, École Polytechnique Fédérale de Lausanne, CH-1015 Lausanne, Switzerland

[||]King Abdullah Institute for Nanotechnology, King Saud University, Riyadh 11451, Saudi Arabia

Ⓢ *Supporting Information*

ABSTRACT: Probing local emission properties of organic−inorganic lead halide perovskite material can provide evidence regarding the photovoltaic performance of perovskite solar cells. Herein, cathodoluminescence, which has the potential to resolve emission characteristics in the nanoregime, has been exploited to carry out temperature-dependent studies on individual well-faceted $CH_3NH_3PbI_{3−x}Br_x$ perovskite single crystals. The spatial distribution of emission recorded at 4 and 300 K reveals that the periphery of the perovskite crystals radiates predominantly, which establishes that such an unusual emission characteristic is independent of the crystallographic phase of $CH_3NH_3PbI_{3−x}Br_x$ crystals. Investigation based on scanning transmission electron microscopy coupled with energy dispersive X-ray spectroscopy deduces that the asymmetric cathodoluminescence is associated with the nonhomogeneous distribution of methylammonium cations in $CH_3NH_3PbI_{3−x}Br_x$ single crystals. These results emphasize the unraveling of a correlation between the composition and spectroscopic properties of perovskite crystals in the nanoregime, which eventually can influence the overall photovoltaic performance of the devices based on them.

KEYWORDS: *cathodoluminescence, $CH_3NH_3PbI_{3−x}Br_x$ perovskite, single crystal, transmission electron microscopy, EDS mapping*
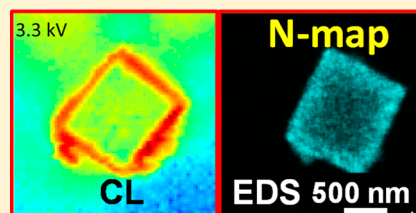
Quantum efficiency of luminescence under both short-circuit and open-circuit conditions provides direct evidence regarding the efficiency of a solar cell or a light-emitting device.[1] In fact, investigating emission properties of a light absorber, such as organic−inorganic lead halide perovskite, can be useful in estimating the power conversion efficiency of a perovskite solar cell.[2,3] Recent unprecedented development in organic−inorganic lead halide perovskite solar cells has received the attention of the photovoltaic community.[4] Kojima et al. were the first to report a power conversion efficiency of 3.8% while using $CH_3NH_3PbI_3$ as light-harnessing material in a liquid electrolyte based sensitized solar cell.[5] Later on, Park and co-workers documented an improved efficiency of 6.5% for a $CH_3NH_3PbI_3$ perovskite device.[6] While retaining the architecture of solid-state dye-sensitized solar cells, subsequently higher efficiencies were reported.[7−10]

Organic−inorganic lead halide perovskites have also been demonstrated as potential candidates in various fields such as light-emitting diodes (LEDs), field effect transistors (FET), and lasers.[11−13] In addition to enticing optical and excitonic properties, the hybrid perovskite materials exhibit strong emission characteristics. Various studies related to spatially resolved emission characteristics of organic−inorganic perovskite semiconductor materials have been carried out; however most of them have focused on polycrystalline film samples.

Using transient absorption microscopy with 50 nm spatial resolution, Guo et al. documented a direct measurement of carrier transport in space and in time by mapping carrier density with simultaneous ultrafast time resolution in perovskite thin films.[14] Photoluminescence decay dynamics resolved using confocal fluorescence microscopy was found to vary between different grains of compositionally nonhomogeneous perovskite films.[15] Widening of the band gap and faster photocarrier recombination at the edge of the $CH_3NH_3PbI_3$ crystal were attributed to the local distortion of the lattice.[16] However, the emission characterization techniques that are commonly used, such as photoluminescence and electroluminescence, are ineffective to resolve spectral features in the nanoregime. Therefore, exploring local emission properties of organic−inorganic lead halide perovskite material can provide further evidence regarding the photovoltaic performance of perovskite solar cells. In $CH_3NH_3PbI_3$ thin films, lateral and depth-dependent variation of the recombination rate at the nanoscale was studied using cathodoluminescence (CL) spectroscopy.[17]

Herein, we have exploited the potential of cathodoluminescence spectroscopy to analyze the local emission characteristics

of $CH_3NH_3PbI_{3-x}Br_x$ single crystals over a temperature range of 4 to 300 K. The $CH_3NH_3PbI_{3-x}Br_x$ crystals were obtained after immersing a $PbBr_2$ film deposited onto mesoporous Al_2O_3 into a solution of CH_3NH_3I for 20 min (Figure 1).[18] Formation

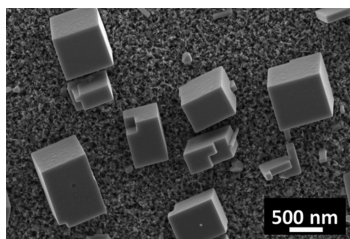**Figure 1.** FESEM micrograph of $CH_3NH_3PbI_{3-x}Br_x$ crystals supported on mesoporous Al_2O_3.

of well-faceted $CH_3NH_3PbI_{3-x}Br_x$ ($x < 2$ atomic %) single crystals with dimension of 1–2 μm was confirmed by field emission secondary electron microscopy (FESEM) and transmission electron microscopy (TEM). Spatially resolved CL emission recorded at 4 and 300 K brings out asymmetric emission in $CH_3NH_3PbI_{3-x}Br_x$ single crystals. Structural, morphological, and elemental analyses based on scanning transmission electron microscopy coupled with energy dispersive X-ray spectroscopy (STEM-EDS) ascribed the asymmetric cathodoluminescence to the nonhomogeneous distribution of methylammonium cations in $CH_3NH_3PbI_{3-x}Br_x$ single crystals. Therefore, understanding a correlation between the composition and properties of perovskite structures in the nanoregime becomes imperative, as it can dictate the overall photovoltaic performance of the solar cell.

Temperature-Dependent Cathodoluminescence. After cooling the $CH_3NH_3PbI_{3-x}Br_x$ crystals to low temperature ($\sim$4 K) CL studies were carried out. Figure 2 shows the

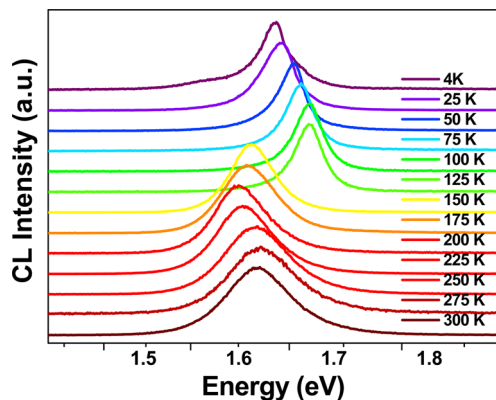**Figure 2.** Temperature-dependent cathodoluminescence spectra recorded from $CH_3NH_3PbI_{3-x}Br_x$ crystals.

temperature-dependent CL spectra recorded from $CH_3NH_3PbI_{3-x}Br_x$ single crystals. At 4 K an emission peak located at 1.62 eV was observed, which displayed a systematic blue-shift when the temperature was increased up to 125 K. By increasing the temperature from 125 to 150 K, a large red-shift in the emission peak position confirming the transition from orthorhombic to tetragonal $CH_3NH_3PbI_{3-x}Br_x$ phase was observed. The presence of a single emission peak around the phase transition temperature (125–150 K) brings out the single-crystalline nature of $CH_3NH_3PbI_{3-x}Br_x$ crystals.[19] Above

175 K, the emission peak revealed a shift toward higher energy up to 300 K. A minor inconsistency observed in the peak shift between 150 and 175 K could be attributed to a variation in the dimensions of $CH_3NH_3PbI_{3-x}Br_x$ crystals chosen for the CL measurement.[20] To avoid the damage induced by the electron beam, different $CH_3NH_3PbI_{3-x}Br_x$ crystals were probed at various temperatures. Overall, the blue-shift infers widening of the band gap in the organic–inorganic perovskites, which is in contrast with the usual Varshni behavior observed in standard tetrahedral semiconductors, as the latter experience a red-shift with the increase in temperature.[21]

Furthermore, the existence of a single CL emission peak at low temperature is in apparent discord with the previous studies involving temperature-dependent photoluminescence studies of perovskites, as all of them reported an additional emission peak below 120 K.[22] Xing et al.[13] observed two additional emission peaks at low temperature, which were attributed to two bound exciton emissions (815 and 782 nm) and a free exciton emission (746 nm), whereas Kong et al. attributed them to a free exciton (higher energy) and a donor–acceptor pair (low energy) transition.[23] Fang et al. attributed the low- and high-energy emission peaks to free and bound excitons, respectively.[24] It is to be noted that all these studies were carried out on polycrystalline samples. On the contrary, our study involves $CH_3NH_3PbI_{3-x}Br_x$ single crystals, which clearly surmises that the origin of the additional peak can also be associated with the crystallinity or nature of the perovskite materials. Moreover, no feature corresponding to PbI_2 was found in the CL spectrum (Figure S1), which amply rules out the decomposition of $CH_3NH_3PbI_{3-x}Br_x$ into PbI_2 under these conditions.[25]

Cathodoluminescence Mapping. The spatial distribution of the emission in $CH_3NH_3PbI_{3-x}Br_x$ single crystals was investigated using CL spectroscopy. Figure 3a shows the secondary electron (SE) image of a $CH_3NH_3PbI_{3-x}Br_x$ crystal with a dimension of 2 μm. CL mapping of the individual $CH_3NH_3PbI_{3-x}Br_x$ crystal acquired at 4 K is shown in Figure 3b. Surprisingly, the spatial distribution of emission shows that the periphery of the $CH_3NH_3PbI_{3-x}Br_x$ crystal is predominantly radiative, whereas the center exhibits a negligible CL emission. We also noticed that the smaller crystals (in the upper left corner of the image in Figure 3b) are relatively more radiative. To rule out that the unusual emission characteristic is not specifically associated with the low-temperature orthorhombic phase, CL mapping measurements were carried out above the phase transition temperature. Figure 3d,e present the SEM image together with the CL intensity mapping integrated between 742 and 793 nm acquired at 300 K. Overall, the spatial distribution of CL emission was found to be consistent with low-temperature measurements, which confirms that non-homogeneous CL emission across perovskite crystals is not associated with the crystallographic phase of $CH_3NH_3PbI_{3-x}Br_x$ crystals. Figure 3c,f display the integrated CL intensity across the two $CH_3NH_3PbI_{3-x}Br_x$ crystals. From these profiles, we can observe that the CL intensity remains insignificant at the center of the perovskite crystals. In fact, at 300 K, the CL intensity decreases by an order of magnitude. It is worth mentioning that the spatial resolution of the cathodoluminescence signal starts where the carriers are generated and not where they recombine. In the CL measurement, the luminescence intensity is correlated with the position of the incident electron beam, and contrary to confocal microscopy, no spatial filtering is performed in the collection line. As a result, if the diffusion
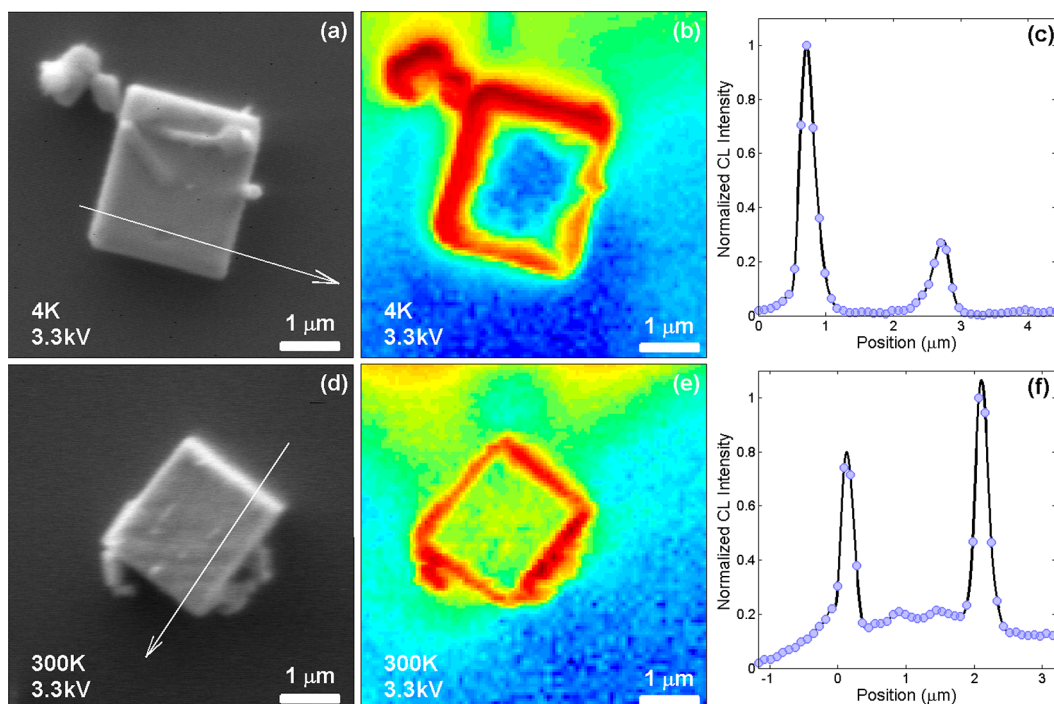
Figure 3. (a) SEM image of a typical $CH_3NH_3PbI_{3-x}Br_x$ single crystal at 4 K. (b) CL mapping acquired at 4 K on the same crystal. The intensity has been integrated between 755 and 765 nm. (c) Line scan recorded along the indicated line over a crystal depicted in (a). (d) SEM image of a typical $CH_3NH_3PbI_{3-x}Br_x$ single crystal at 300 K. (e) CL mapping acquired at 300 K on the same crystal. The intensity has been integrated between 742 and 793 nm. (f) Line scan recorded along the indicated line over a crystal depicted in (d).
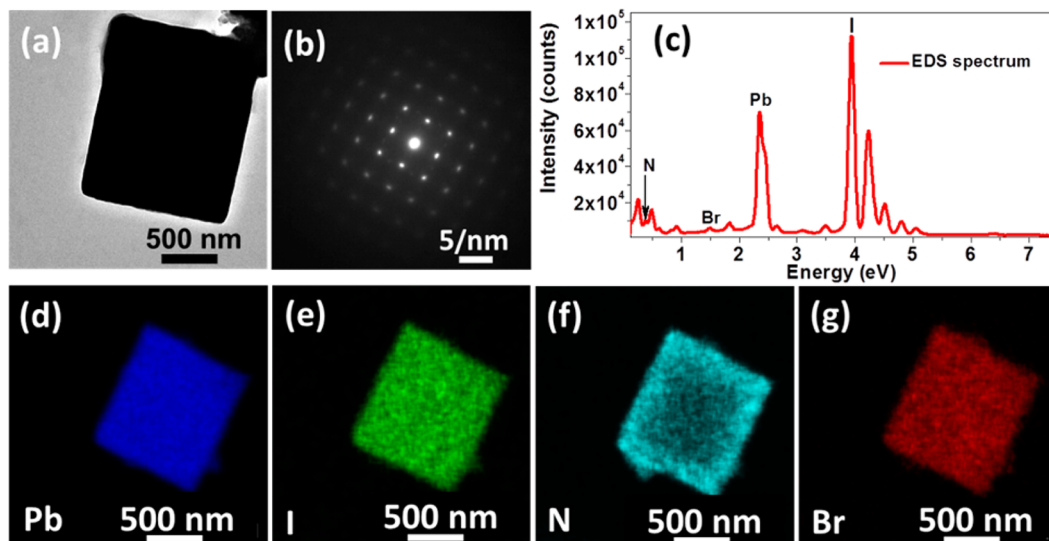

Figure 4. TEM and STEM-EDS analysis of an individual $CH_3NH_3PbI_{3-x}Br_x$ crystal. (a) BFTEM micrograph, (b) SAED pattern, (c) STEM-EDS spectrum, (d) Pb map, (e) I map, (f) N map, and (g) Br map.

length is large enough, we can collect photons emitted far from the incident electron beam.

Furthermore, asymmetric distribution in CL is not merely linked to well-defined $CH_3NH_3PbI_{3-x}Br_x$ crystals with dimension of 1−2 μm, as similar emission characteristics prevailed (Figure S2) when asymmetric but faceted $CH_3NH_3PbI_{3-x}Br_x$ crystals were probed. Enhanced surface emission from the cubic perovskite single crystals originating from the whispering gallery modes (WGMs) has been previously reported.[26] The enhanced surface emission in our $CH_3NH_3PbI_{3-x}Br_x$ crystals cannot be related with WGM

phenomena, as it is also observed in irregular shaped crystals (Figure S2). Recently, Tian et al. observed size-dependent light-induced photoluminescence enhancement in $CH_3NH_3PbI_3$ perovskite crystals and concluded that traps are distributed over the entire perovskite crystal volume.[27] From grain to grain, a variation in the photoluminescence has been observed within the same perovskite film, and due to the faster nonradiative recombination, the grain boundaries were found to be dimmer.[15] Surprisingly, we observe a very intense emission from the periphery of the $CH_3NH_3PbI_{3-x}Br_x$ crystals. It is well known that the photophysical properties strongly depend on

the growth, crystallinity, and composition of the perovskite materials.[28] Such a spatial variation in CL (Figure 3b,e) observed in $CH_3NH_3PbI_{3-x}Br_x$ crystals at different temperatures emphasizes the significance of determining the composition and distribution of elements in the nanoregime.[29] Therefore, analyzing the composition of the $CH_3NH_3PbI_{3-x}Br_x$ crystal became essential and was carried out using STEM-EDS.

Electron Microscopy. TEM was used to examine the morphology, dimension, and crystallinity of the $CH_3NH_3PbI_{3-x}Br_x$ perovskite crystals. The bright-field TEM (BFTEM) image (Figure 4a) shows the formation of a well-faceted $CH_3NH_3PbI_{3-x}Br_x$ crystal with a diameter of 1 μm, which is in agreement with FESEM analysis. Selected area electron diffraction (SAED) displays a bright spot pattern (Figure 4b) indexable to the tetragonal phase of $CH_3NH_3PbI_3$, which further confirms the single-crystalline nature of $CH_3NH_3PbI_{3-x}Br_x$ crystals.

In this study, as the preparation of $CH_3NH_3PbI_{3-x}Br_x$ single crystals involved a conversion reaction between $PbBr_2$ and CH_3NH_3I, the analysis of halide composition and distribution of constituent elements became important and was carried out by performing EDS mapping under STEM mode on individual $CH_3NH_3PbI_{3-x}Br_x$ crystals. The STEM-EDS spectrum (Figure 4c) shows that Pb, I, N, and Br are present in a $CH_3NH_3PbI_{3-x}Br_x$ single crystal. Although the conversion reaction involves pure $PbBr_2$, a mild feature (<2 at. %) corresponding to bromide was present in the EDS spectrum (Figure 4c). The formation of iodide-dominant $CH_3NH_3PbI_{3-x}Br_x$ crystals could be explained by invoking the phenomenon of halide exchange (bromide by iodide of CH_3NH_3I).[18] Previously, under continuous illumination, an additional PL peak at 1.68 eV was observed in $CH_3NH_3Pb(I_{1-x}Br_x)_3$ (0.2 < x > 1), which has been attributed to the existence of multiple phases of mixed halide perovskites.[30,31] In our case, the content of bromide in $CH_3NH_3PbI_{3-x}Br_x$ crystals is marginal ([Br] < 2 at. %), which in combination with the presence of a single CL emission peak (Figure 2) rules out the possibility of segregation of iodide-rich and bromide-rich phases under the electron beam. Area mapping under the STEM-EDS mode was further carried out to locate the constituent elements in the nanoregime, as their spatial distribution can critically influence the photophysical properties of perovskite structures.[15] STEM-EDS mapping provided direct evidence of the uniform distribution of Pb, I, and Br throughout the dimension of the $CH_3NH_3PbI_{3-x}Br_x$ crystal (Figure 4d−g); however, the distribution of N (methylammonium cation) was found to be inhomogeneous. The intensity of the N signal is stronger toward the periphery of the $CH_3NH_3PbI_{3-x}Br_x$ crystal, so we could envisage a gradient/inhomogeneity in the band gap across the dimension of the $CH_3NH_3PbI_{3-x}Br_x$ crystal. Possibly, the central part of the $CH_3NH_3PbI_{3-x}Br_x$ crystal exhibits a relatively wider band gap (CH_3NH_3-deficient region). From our CL and STEM investigation, we surmise that the phenomenon of halide exchange observed in hybrid perovskites can bring inhomogeneity in the distribution of constituents and emission at a submicroscopic level. Therefore, investigation of the distribution of constituent elements in various perovskite structures obtained, specifically through halide exchange, becomes imperative. More mechanistic studies regarding the process of self-absorption and inhomogeneous distribution of CH_3NH_3 cations in $CH_3NH_3PbBr_xI_{3-x}$ structures need to be carried out. In addition, it would be worth exploring well-formed crystals of pure iodide- and bromine-based perovskites.

In summary, cathodoluminescence spectroscopy in combination with scanning transmission electron microscopy and energy dispersive X-ray spectroscopy analysis in the nanoregime revealed that the asymmetric emission is associated with the nonhomogeneous distribution of CH_3NH_3 cations in $CH_3NH_3PbBr_xI_{3-x}$ single crystals. This work emphasizes the unraveling of a correlation between the growth, composition, and spectroscopic properties of perovskite crystals in the nanoregime, which arguably dictate the overall performance of the device.[32,33]

■ EXPERIMENTAL SECTION

Preparation of Samples. Fluorine-doped tin oxide (FTO) (NSG 10, Nippon Sheet Glass, Japan) substrate was cleaned with a detergent, rinsed with deionized water and ethanol, and then treated in a UV/O_3 cleaner for 10 min. A 250 nm thick Al_2O_3 mesoporous layer was deposited on the precleaned FTO glass substrate by spin coating a diluted paste (1:3.5 wt ratio) (30 nm Al_2O_3) (5000 rpm, acceleration 2000 rpm for 30 s). After sintering at 450 °C for 30 min with a 10 min ramp time, mesoporous Al_2O_3 films were obtained. All materials were purchased from Sigma-Aldrich and were used as received. A 1.2 M solution of $PbBr_2$ was prepared in dimethyl sulfoxide (DMSO) solvent by constant stirring at 80 °C for 30 min. $PbBr_2$ was deposited onto mesoporous Al_2O_3 films by spin-coating the $PbBr_2$ solution at 3000 rpm for 30 s and dried at 80 °C for 15 min. After cooling to room temperature, perovskite crystals were obtained by immersing the resulting $PbBr_2$ films into a solution of CH_3NH_3I in 2-propanol (8 mg mL^{-1}) for 20 min and were subsequently dried at 80 °C for 15 min. For the deposition of $CH_3NH_3PbI_3$, a two-step approach was used. A 50 μL amount of a 1.2 M solution of PbI_2 in dimethylformamide was deposited onto mesoporous Al_2O_3 films by spin-coating at 3000 rpm for 30 s and dried at 80 °C for 15 min. After cooling to room temperature, $CH_3NH_3PbI_3$ films were obtained by immersing the resulting PbI_2 films into a solution of CH_3NH_3I in 2-propanol (8 mg mL^{-1}) for 2 min and were subsequently dried at 80 °C for 15 min.

Cathodoluminescence. Cathodoluminescence spectroscopy measurements were performed using an Attolight Alalin Chronos 4027 system, working in continuous operation mode. A probe current of 2 nA and acceleration voltage of 3.3 kV were selected as a result of a trade-off between spatial resolution and CL signal intensity. The dwell time of 10 ms at 4 K and 50 ms at 300 K was chosen for acquiring the data. The CL specimens were prepared by slow evaporation of diluted solutions, obtained by dispersion of perovskite powders in toluene, and deposited on a silicon substrate. The powder was obtained after scratching the perovskite film from the substrate.

Electron Microscopy. A field-emission scanning electron microscope (Merlin) was employed to analyze the morphology of the film sample. An electron beam accelerated to 3 kV was used with an in-lens detector. The perovskite crystals were examined by an Osiris field-emission transmission electron microscope operating at an accelerating voltage of 200 kV, equipped with an Oxford energy-dispersive X-ray detector. The TEM specimens were prepared by slow evaporation of diluted solutions, obtained by dispersion of perovskite powder by sonication in toluene, and deposited on a Formvar-coated carbon copper grid. The perovskite powder was obtained after scratching the film from the substrate.

■ ASSOCIATED CONTENT

Ⓢ Supporting Information

The Supporting Information is available free of charge on the ACS Publications website at DOI: 10.1021/acsphotonics.6b00290.

FESEM, STEM, and CL analysis of $CH_3NH_3PbI_{3-x}Br_x$ crystals (PDF)

■ AUTHOR INFORMATION

Corresponding Author
*E-mail: ibrahim.dar@epfl.ch. Fax: (+) 41-21 693 6100.

Author Contributions
#M. I. Dar and G. Jacopin contributed equally.

Notes
The authors declare no competing financial interest.

■ ACKNOWLEDGMENTS

■ REFERENCES

(1) Tvingstedt, K.; Malinkiewicz, O.; Baumann, A.; Deibel, C.; Snaith, H. J.; Dyakonov, V.; Bolink, H. J. Radiative efficiency of lead iodide based perovskite solar cells. *Sci. Rep.* **2014**, *4*, 6071.

(2) Rau, U. Reciprocity relation between photovoltaic quantum efficiency and electroluminescent emission of solar cells. *Phys. Rev. B: Condens. Matter Mater. Phys.* **2007**, *76*, 085303.

(3) Tress, W.; Marinova, N.; Inganäs, O.; Nazeeruddin, M. K.; Zakeeruddin, S. M.; Graetzel, M. Predicting the Open-Circuit Voltage of $CH_3NH_3PbI_3$ Perovskite Solar Cells Using Electroluminescence and Photovoltaic Quantum Efficiency Spectra: The Role of Radiative and Non-Radiative Recombination. *Adv. Energy Mater.* **2015**, *5*, 1400812.

(4) Gratzel, M. The Light and Shade of Perovskite Solar Cells. *Nat. Mater.* **2014**, *13*, 838−842.

(5) Kojima, A.; Teshima, K.; Shirai, Y.; Miyasaka, T. Organometal Halide Perovskites as Visible-Light Sensitizers for Photovoltaic Cells. *J. Am. Chem. Soc.* **2009**, *131*, 6050−6051.

(6) Im, J.-H.; Lee, C.-R.; Lee, J.-W.; Park, S.-W.; Park, N.-G. 6.5% Efficient Perovskite Quantum-Dot-Sensitized Solar Cell. *Nanoscale* **2011**, *3*, 4088−4093.

(7) Kim, H.-S.; Lee, C.-R.; Im, J.-H.; Lee, K.-B.; Moehl, T.; Marchioro, A.; Moon, S.-J.; Humphry-Baker, R.; Yum, J.-H.; Moser, J. E.; Grätzel, M.; Park, N.-G. Lead Iodide Perovskite Sensitized All-Solid-State Submicron Thin Film Mesoscopic Solar Cell with Efficiency Exceeding 9%. *Sci. Rep.* **2012**, *2*, 591.

(8) Lee, M. M.; Teuscher, J.; Miyasaka, T.; Murakami, T. N.; Snaith, H. J. Efficient Hybrid Solar Cells Based on Meso-Superstructured Organometal Halide Perovskites. *Science* **2012**, *338*, 643−647.

(9) Burschka, J.; Pellet, N.; Moon, S.-J.; Humphry-Baker, R.; Gao, P.; Nazeeruddin, M. K.; Gratzel, M. Sequential Deposition as a Route to High-Performance Perovskite-Sensitized Solar Cells. *Nature* **2013**, *499*, 316−319.

(10) Jeon, N. J.; Noh, J. H.; Yang, W. S.; Kim, Y. C.; Ryu, S.; Seo, J.; Seok, S. I. Compositional Engineering of Perovskite Materials for High-Performance Solar Cells. *Nature* **2015**, *517*, 476−480.

(11) Kagan, C. R.; Mitzi, D. B.; Dimitrakopoulos, C. D. Organic-Inorganic Hybrid Materials as Semiconducting Channels in Thin-Film Field-Effect Transistors. *Science* **1999**, *286*, 945−947.

(12) Tan, Z.-K.; Moghaddam, R. S.; Lai, M. L.; Docampo, P.; Higler, R.; Deschler, F.; Price, M.; Sadhanala, A.; Pazos, L. M.; Credgington, D.; Hanusch, F.; Bein, T.; Snaith, H. J.; Friend, R. H. Bright light-emitting diodes based on organometal halide perovskite. *Nat. Nanotechnol.* **2014**, *9*, 687−692.

(13) Xing, G.; Mathews, N.; Lim, S. S.; Yantara, N.; Liu, X.; Sabba, D.; Grätzel, M.; Mhaisalkar, S.; Sum, T. C. Low-Temperature Solution-Processed Wavelength-Tunable Perovskites for Lasing. *Nat. Mater.* **2014**, *13*, 476−480.

(14) Guo, Z.; Manser, J. S.; Wan, Y.; Kamat, P. V.; Huang, L. Spatial and Temporal Imaging of Long-Range Charge Transport in Perovskite Thin Films by Ultrafast Microscopy. *Nat. Commun.* **2015**, *6*, 7471.

(15) de Quilettes, D. W.; Vorpahl, S. M.; Stranks, S. D.; Nagaoka, H.; Eperon, G. E.; Ziffer, M. E.; Snaith, H. J.; Ginger, D. S. Impact of Microstructure on Local Carrier Lifetime in Perovskite Solar Cells. *Science* **2015**, *348*, 683−686.

(16) Grancini, G.; D'Innocenzo, V.; Dohner, E. R.; Martino, N.; Srimath Kandada, A. R.; Mosconi, E.; De Angelis, F.; Karunadasa, H. I.; Hoke, E. T.; Petrozza, A. $CH_3NH_3PbI_3$ Perovskite Single Crystals: Surface Photophysics and Their Interaction with the Environment. *Chem. Sci.* **2015**, *6*, 7305−7310.

(17) Bischak, C. G.; Sanehira, E. M.; Precht, J. T.; Luther, J. M.; Ginsberg, N. S. Heterogeneous Charge Carrier Dynamics in Organic−Inorganic Hybrid Materials: Nanoscale Lateral and Depth-Dependent Variation of Recombination Rates in Methylammonium Lead Halide Perovskite Thin Films. *Nano Lett.* **2015**, *15*, 4799−4807.

(18) Dar, M. I.; Abdi-Jalebi, M.; Arora, N.; Moehl, T.; Grätzel, M.; Nazeeruddin, M. K. Understanding the Impact of Bromide on the Photovoltaic Performance of $CH_3NH_3PbI_3$ Solar Cells. *Adv. Mater.* **2015**, *27*, 7221−7228.

(19) D'Innocenzo, V.; Grancini, G.; Alcocer, M. J. P.; Kandada, A. R. S.; Stranks, S. D.; Lee, M. M.; Lanzani, G.; Snaith, H. J.; Petrozza, A. Excitons Versus Free Charges in Organo-Lead Tri-Halide Perovskites. *Nat. Commun.* **2014**, *5*, 3586.

(20) D'Innocenzo, V.; Srimath Kandada, A. R.; De Bastiani, M.; Gandini, M.; Petrozza, A. Tuning the Light Emission Properties by Band Gap Engineering in Hybrid Lead Halide Perovskite. *J. Am. Chem. Soc.* **2014**, *136*, 17730−17733.

(21) Varshni, Y. P. Temperature Dependence of the Energy Gap in Semiconductors. *Physica* **1967**, *34*, 149−154.

(22) Wu, K.; Bera, A.; Ma, C.; Du, Y.; Yang, Y.; Li, L.; Wu, T. Temperature-Dependent Excitonic Photoluminescence of Hybrid Organometal Halide Perovskite Films. *Phys. Chem. Chem. Phys.* **2014**, *16*, 22476−22481.

(23) Kong, W.; Ye, Z.; Qi, Z.; Zhang, B.; Wang, M.; Rahimi-Iman, A.; Wu, H. Characterization of an Abnormal Photoluminescence Behavior Upon Crystal-Phase Transition of Perovskite $CH_3NH_3PbI_3$. *Phys. Chem. Chem. Phys.* **2015**, *17*, 16405−16411.

(24) Fang, H.-H.; Raissa, R.; Abdu-Aguye, M.; Adjokatse, S.; Blake, G. R.; Even, J.; Loi, M. A. Photophysics of Organic−Inorganic Hybrid Lead Iodide Perovskite Single Crystals. *Adv. Funct. Mater.* **2015**, *25*, 2378−2385.

(25) Xiao, C.; Li, Z.; Guthrey, H.; Moseley, J.; Yang, Y.; Wozny, S.; Moutinho, H.; To, B.; Berry, J. J.; Gorman, B.; Yan, Y.; Zhu, K.; Al-Jassim, M. Mechanisms of Electron-Beam-Induced Damage in Perovskite Thin Films Revealed by Cathodoluminescence Spectroscopy. *J. Phys. Chem. C* **2015**, *119*, 26904−26911.

(26) Liao, Q.; Hu, K.; Zhang, H.; Wang, X.; Yao, J.; Fu, H. Perovskite Microdisk Microlasers Self-Assembled from Solution. *Adv. Mater.* **2015**, *27*, 3405−3410.

(27) Tian, Y.; Merdasa, A.; Unger, E.; Abdellah, M.; Zheng, K.; McKibbin, S.; Mikkelsen, A.; Pullerits, T.; Yartsev, A.; Sundström, V.; Scheblykin, I. G. Enhanced Organo-Metal Halide Perovskite Photoluminescence from Nanosized Defect-Free Crystallites and Emitting Sites. *J. Phys. Chem. Lett.* **2015**, *6*, 4171−4177.

(28) Dar, M. I.; Arora, N.; Gao, P.; Ahmad, S.; Grätzel, M.; Nazeeruddin, M. K. Investigation Regarding the Role of Chloride in Organic−Inorganic Halide Perovskites Obtained from Chloride Containing Precursors. *Nano Lett.* **2014**, *14*, 6991−6996.

(29) Hentz, O.; Zhao, Z.; Gradečak, S. Impacts of Ion Segregation on Local Optical Properties in Mixed Halide Perovskite Films. *Nano Lett.* **2016**, *16*, 1485−1490.

(30) Hoke, E. T.; Slotcavage, D. J.; Dohner, E. R.; Bowring, A. R.; Karunadasa, H. I.; McGehee, M. D. Reversible Photo-Induced Trap Formation in Mixed-Halide Hybrid Perovskites for Photovoltaics. *Chem. Sci.* **2015**, *6*, 613−617.

(31) Sadhanala, A.; Deschler, F.; Thomas, T. H.; Dutton, S. E.; Goedel, K. C.; Hanusch, F. C.; Lai, M. L.; Steiner, U.; Bein, T.; Docampo, P.; Cahen, D.; Friend, R. H. Preparation of Single-Phase Films of $CH_3NH_3Pb(I_{1-x}Br_x)_3$ with Sharp Optical Band Edges. *J. Phys. Chem. Lett.* **2014**, *5*, 2501−2505.

(32) Arora, N.; Dar, M. I.; Hezam, M.; Tress, W.; Jacopin, G.; Moehl, T.; Gao, P.; Aldwayyan, A. S.; Deveaud, B.; Gratzel, M.; et al. Photovoltaic and Amplified Spontaneous Emission Studies of High Quality Formamidinium Lead Bromide Perovskite Films. *Adv. Funct. Mater.* **2016**, *26*, 2846−2854.

(33) Dar, M. I.; Abdi-Jalebi, M.; Arora, N.; Grätzel, M.; Nazeeruddin, M. K. Growth Engineering of $CH_3NH_3PbI_3$ Structures for High-Efficiency Solar Cells. *Adv. Energy Mater.* **2016**, *6*, 1501358.